30 August 2026

Compositional Disorder Controls Bulk Ion Diffusion in Mixed-Ion Halide Perovskites

Benjamin M. Gallant[1], Priyanka Deswal[2], Shrestha Banerjee[1], Erik Fransson[2], Jem Hammerton[3], Michael Walters[1], Joshua Deakin[1], William Burston[1], Paul Erhart[2], Julia Wiktor[2], Dominik J. Kubicki[1]

1. School of Chemistry, University of Birmingham

2. Department of Physics and Astronomy, Chalmers University of Technology

3. School of Metallurgy and Materials, University of Birmingham

Abstract

Compositional mixing enables bandgap and phase-stability engineering in metal halide perovskites, but its effect on intrinsic ion mobility is obscured by surfaces, interfaces, and concurrent structural dynamics. Here, variable-temperature magic-angle-spinning NMR combined with machine-learning-accelerated molecular dynamics separates soft-phonon relaxation from vacancy-mediated diffusion across a Cs/Rb–Br/I composition matrix. Br/I mixing markedly accelerates bulk halide transport, whereas combined Br/I and Cs/Rb substitution produces a second, slower regime assigned to A-site cation diffusion. Linewidth and relaxation analyses yield consistent hopping barriers and an Arrhenius-extrapolated room-temperature bulk halide diffusivity of order 10−11 cm2 s−1, below values commonly inferred from electrical measurements of thin films. Simulations at fixed vacancy concentration reproduce the species-dependent mobility trends and indicate that static local distortions broaden the distribution of migration environments, creating locally accessible pathways for ion motion. These results distinguish intrinsic mobility per available defect from macroscopic ion redistribution, which additionally depends on defect abundance, interfaces, and thermodynamic or photoinduced driving forces. Enhanced per-defect mobility therefore need not imply rapid operational phase segregation, providing a framework for connecting compositional disorder with processing and stability in multicomponent ionic semiconductors.

Compositional Disorder Controls Bulk Ion Diffusion in Mixed-Ion Halide Perovskites

Benjamin M. Gallant[1], Priyanka Deswal[2], Shrestha Banerjee[1], Erik Fransson[2], Jem Hammerton[3], Michael Walters[1], Joshua Deakin[1], William Burston[1], Paul Erhart[2], Julia Wiktor[2], Dominik J. Kubicki[1]*

[1]School of Chemistry, University of Birmingham; Birmingham, B15 2TT, United Kingdom

[2]Department of Physics and Astronomy, Chalmers University of Technology; Gothenburg, SE-41296, Sweden

[3]School of Metallurgy and Materials, University of Birmingham; Birmingham, B15 2TT, United Kingdom.

ABSTRACT: Compositional mixing enables bandgap and phase-stability engineering in metal halide perovskites, but its effect on intrinsic ion mobility is obscured by surfaces, interfaces, and concurrent structural dynamics. Here, variable-temperature magic-angle-spinning NMR combined with machine-learning-accelerated molecular dynamics separates soft-phonon relaxation from vacancy-mediated diffusion across a Cs/Rb–Br/I composition matrix. Br/I mixing markedly accelerates bulk halide transport, whereas combined Br/I and Cs/Rb substitution produces a second, slower regime assigned to A-site cation diffusion. Linewidth and relaxation analyses yield consistent hopping barriers and an Arrhenius-extrapolated room-temperature bulk halide diffusivity of order 10^{-11} cm^2 s^{-1}, below values commonly inferred from electrical measurements of thin films. Simulations at fixed vacancy concentration reproduce the species-dependent mobility trends and indicate that static local distortions broaden the distribution of migration environments, creating locally accessible pathways for ion motion. These results distinguish intrinsic mobility per available defect from macroscopic ion redistribution, which additionally depends on defect abundance, interfaces, and thermodynamic or photoinduced driving forces. Enhanced per-defect mobility therefore need not imply rapid operational phase segregation, providing a framework for connecting compositional disorder with processing and stability in multicomponent ionic semiconductors.

Atomic-level motion in metal halide perovskites underlies both the promise and the instability of these semiconductors. Their unusual defect tolerance, long carrier lifetimes, and compositional tunability have made halide perovskites central to emerging optoelectronic technologies, especially multi-junction photovoltaics (PVs).[1–3] Yet the same compositional flexibility that enables control over bandgap and phase stability also creates pathways for local phase segregation and to transformation into photoinactive non-perovskite phases under operating conditions.[1,3–6] These trade-offs are especially acute in Cs^+-containing mixed bromide-iodide compositions with bandgaps near 2 eV, which now play a key role in high-efficiency multi-junction PV devices.[1,7,8] A central challenge is that the thermal behavior of these materials is governed by several dynamic processes at once, most prominently soft phonon modes associated with octahedral tilting [9] and the diffusion of mobile ions.[10] Both processes are thermally activated, both are strongly composition-dependent, and both reshape structure and performance during synthesis and operation. Yet they have proven difficult to isolate experimentally in the bulk perovskite phase, where the microscopic origin of atomic motion remains incompletely understood. An important distinction is that macroscopic ion redistribution is governed not only by the mobility of individual defects, but also by their concentration, interfaces, and chemical or photoinduced driving forces. Direct measurement of bulk atomic motion is therefore required to separate intrinsic mobility from operational phase segregation.

Most experimental approaches to ion migration in halide perovskites interrogate materials using electrical measurements, where extracted transport parameters are strongly influenced by surfaces, interfaces, and grain boundaries.[11–15] Those measurements are invaluable for device operation[16,17], but they do not necessarily reveal the atomic-scale diffusion processes occurring within the perovskite structure itself, which are crucial for both material synthesis and stability.[1,3] By contrast, magic-angle spinning nuclear magnetic resonance (MAS NMR) directly probes the local environments and dynamics of nuclei throughout the bulk phase. Here we use variable-temperature MAS NMR, combined with molecular dynamics (MD) based on a machine-learned interatomic potential, to disentangle phonon-driven phase behavior from ionic diffusion in a series of inorganic halide perovskites relevant to multi-junction PV: $CsPbBr_3$, $CsPb(Br_{0.5}I_{0.5})_3$, $(Cs_{0.75}Rb_{0.25})PbBr_3$, and $(Cs_{0.75}Rb_{0.25})Pb(Br_{0.5}I_{0.5})_3$. Across this composition series, we show that Br/I mixing accelerates bulk halide transport, whereas combined Br/I and Cs/Rb substitution gives rise to a second, slower A-site diffusion regime. Molecular dynamics reproduces these species-dependent trends at fixed vacancy concentration and indicates that compositional disorder broadens the distribution of local migration environments. This comparison separates intrinsic bulk mobility

from the additional factors governing macroscopic ion redistribution and provides a more rigorous basis for connecting atomic-scale dynamics with the processing and stability of multicomponent halide perovskites.

Separating Phase-Transition Signatures from Diffusive Motion

We first establish how variable-temperature ^{133}Cs MAS NMR captures phase-transition behavior and the underlying phonon dynamics occurring around phase transitions. In these perovskites, ^{133}Cs is highly sensitive to the local structural environment around the A-site and therefore provides a direct probe of thermally induced structural evolution (**Fig. 1a-e** and **Supplementary Note S1**).[1,18,19] For $CsPbBr_3$, the temperature dependence of the isotropic ^{133}Cs shift and linewidth reveals two known phase transitions and supports the existence of an additional low-temperature transition previously proposed from diffraction.[20] The sensitivity of the ^{133}Cs line shape to these subtle structural changes highlights the power of MAS NMR to detect symmetry-breaking behavior that can be difficult to resolve in mixed and disordered materials. However, once compositional mixing is introduced, static disorder substantially broadens the room-temperature ^{133}Cs resonances, masking some of the spectral discontinuities that would otherwise mark phase transitions directly. That broadening is itself informative: it reflects a distribution of local environments created by A-site or X-site substitution. But it also means that a more disorder-tolerant NMR observable is needed to follow phonon-driven transitions across the full composition series.

We therefore turn to ^{133}Cs spin-lattice (T_1) relaxation. As T_1 relaxation is most efficient when atomic motion occurs near the Larmor frequency, minima in T_1 provide a sensitive signature of thermally activated dynamics (**Supplementary Note S2**). In all four compositions, T_1 reveals distinct minima associated with structural phase transitions, although these are not observed for every phase transition (**Fig. 1f–i** and **Supplementary Note S2**). For the three materials in which the high-temperature transition can already be assigned from one-dimensional spectra, the transition temperatures coincide with T_1 minima. For $(Cs_{0.75}Rb_{0.25})Pb(Br_{0.5}I_{0.5})_3$, where static disorder makes straightforward spectral assignment difficult, T_1 clearly captures the high-temperature transition (**Fig. 1i**). These measurements show that relaxation resolves phase behavior even when line broadening obscures it in one-dimensional spectra. This finding is notable as compositional mixing in halide perovskites often makes detecting phase transitions *via* conventional thermal methods challenging.[21,22] More importantly, these NMR relaxation measurements provide a route to isolate phonon-driven phenomena from diffusive motion later in our analysis.

To understand the origin of the strong composition dependence of these transitions, we model the same materials using MD simulations and a machine-learned interatomic potential (**Fig. 1j** and **Supplementary Note S3**).[9] The simulations reproduce the experimentally observed compositional trend in transition temperatures, most notably the marked increase in the high-temperature transition upon partial substitution of Cs^+ by Rb^+. We then analyze the soft phonon modes associated with octahedral tilting. In $CsPbBr_3$, both the M- and R-point tilt modes soften toward the transition as expected, confirming that the observed relaxation minima are coupled to phonon softening. Across the mixed-ion compositions, the same general behavior persists, but the oscillations become more strongly damped and the mode frequencies are reduced. The in-phase M mode is particularly affected, consistent with this mode approaching the ^{133}Cs Larmor frequency closely enough to dominate relaxation near the transition. Together, these results identify the phase-transition signatures that must be distinguished from diffusion-related relaxation in the analysis below. They also show that compositional mixing modifies the phonon spectrum; their principal role here is to provide an internal assignment framework for the subsequent ion-transport measurements.

Compositional Mixing Activates Distinct Halide and A-Site Diffusion Regimes

Having separated phase-transition signatures from other temperature-dependent phenomena, we next examine ion diffusion. Vacancy-mediated hopping is expected to dominate self-diffusion in halide perovskites, with halide motion generally occurring more readily than A-site cation motion.[10,23,24] In $CsPbBr_3$, variable-temperature ^{207}Pb MAS NMR provides an early indication of rapidly changing dynamics: scalar (J) coupling between lead and bromine disappears at elevated temperatures, indicating loss of a static Pb-Br bonding environment on the NMR timescale (**Fig. 2a** and **Supplementary Note S4**). In mixed-ion compositions, however, the most informative probe is again ^{133}Cs NMR. Static disorder broadens the room-temperature ^{133}Cs spectrum because halide or A-site substitution produces a distribution of distinct local Cs^+ environments. When diffusion becomes rapid, that disorder is motionally averaged and the line narrows. This makes line narrowing a sensitive, bulk-selective reporter of species-resolved ion motion in mixed perovskites (**Fig. 2b**).

In $CsPb(Br_{0.5}I_{0.5})_3$, the ^{133}Cs signal, which is broad at room temperature, narrows very substantially on heating, yielding an activation energy for halide hopping of about 0.34 eV *via* linewidth analysis (**Fig. 2c** and **Supplementary Note S4**). In $(Cs_{0.75}Rb_{0.25})PbBr_3$, A-site disorder also broadens the low-temperature signal, but narrowing remains incomplete even at the highest temperatures measured, indicating that A-site diffusion is still comparatively slow (**Fig. 2d**). By contrast, the doubly mixed composition, $(Cs_{0.75}Rb_{0.25})Pb(Br_{0.5}I_{0.5})_3$, undergoes nearly complete narrowing at high temperature despite its much broader room-temperature ^{133}Cs linewidth. In this material, line narrowing occurs in two temperature regimes, corresponding to two independently resolved motional averaging processes (**Fig. 2e, f**). The lower-temperature regime yields the same halide activation energy found for $CsPb(Br_{0.5}I_{0.5})_3$, suggesting halide diffusion is largely insensitive to A-site composition. The higher-temperature regime yields an A-site hopping barrier of around 0.8 eV, which we attribute to motion in the A-site sublattice. These observations collectively show that in this system halide mixing accelerates both halide *and* A-site diffusion.

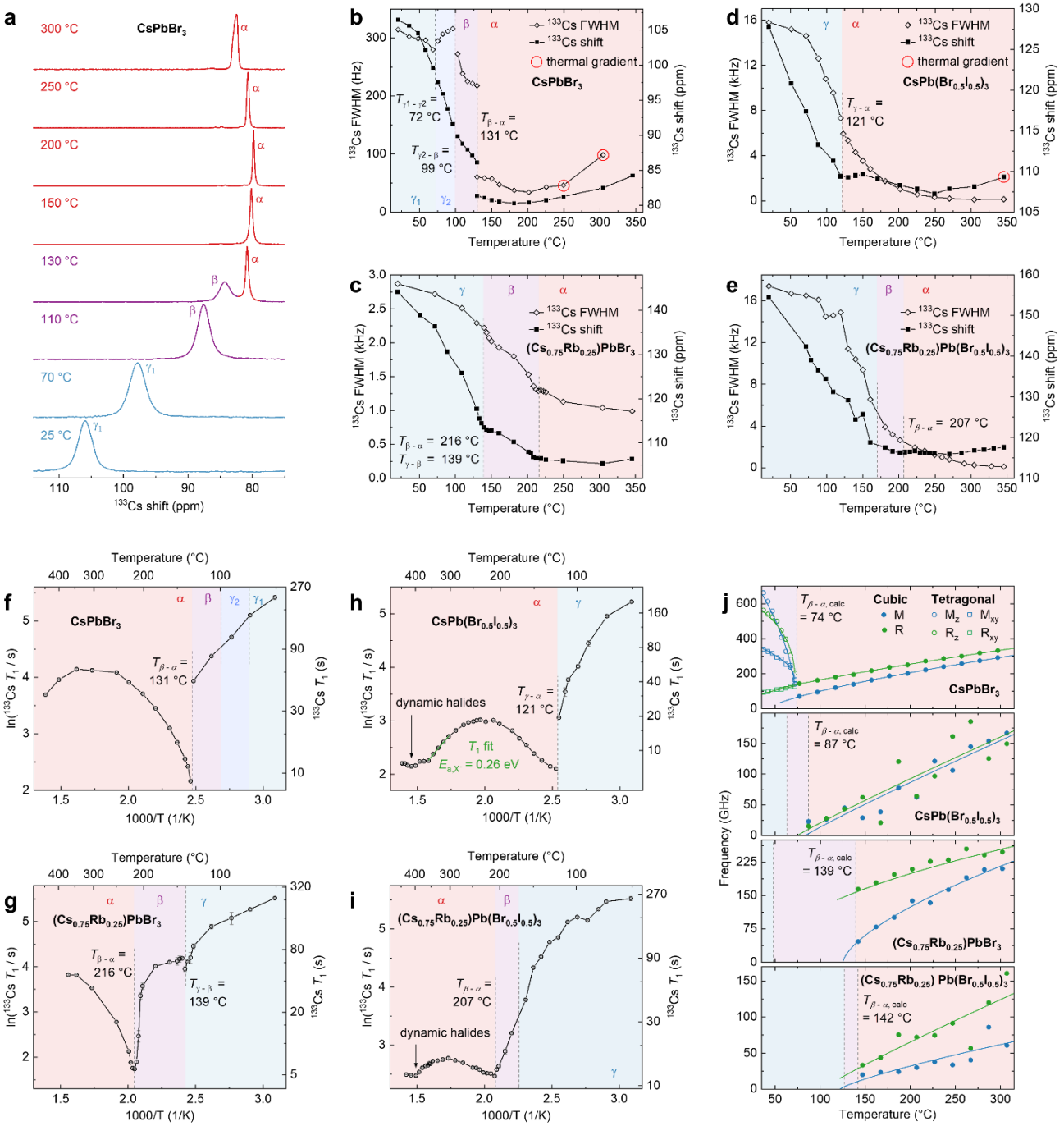

Fig. 1. ^{133}Cs MAS NMR spectroscopy reveals phonon mode softening driving perovskite phase transitions. (**a**) Variable temperature ^{133}Cs MAS NMR spectra (20.0 T, 4 kHz MAS) of $CsPbBr_3$. Summary of ^{133}Cs shift and ^{133}Cs full-width half maximum (FWHM) linewidth extracted from ^{133}Cs MAS NMR of $CsPbBr_3$ (**b**), $(Cs_{0.75}Rb_{0.25})PbBr_3$ (**c**), $CsPb(Br_{0.5}I_{0.5})_3$ (**d**) and $(Cs_{0.75}Rb_{0.25})Pb(Br_{0.5}I_{0.5})_3$ (**e**). (**f-i**) Arrhenius plots of ^{133}Cs T_1 relaxation times for the same four perovskite compositions. Phase transition temperatures are assigned based on NMR spectra wherever possible, or otherwise *via* differential scanning calorimetry measurements (**Fig. S6**). (**j**) M- and R-tilt mode frequencies obtained from MD simulations *via* phonon mode projection analysis as a function of temperature in the tetragonal and cubic phases of inorganic halide perovskites. Solid lines show fits to a Curie-Weiss-type power law as a guide to the eye (see Methods).

^{133}Cs T_1 provides an independent probe of the faster end of this motion. In the two mixed-halide compositions, but not in the bromide-only materials, T_1 exhibits a second high-temperature minimum that does not correspond to a phase transition. For ^{133}Cs at 20 T, this minimum corresponds to motion on the nanosecond timescale and therefore is most consistently attributed to halide diffusion. The fact that the minimum appears at nearly the same temperature in $CsPb(Br_{0.5}I_{0.5})_3$ and $(Cs_{0.75}Rb_{0.25})Pb(Br_{0.5}I_{0.5})_3$ reinforces the conclusion from linewidth analysis that halide diffusion depends primarily on X-site rather than A-site composition. The activation energy obtained from the slope of the

relaxation data is slightly lower compared to that obtained from linewidths (see **Supplementary Note S4-5** for numerical values), but both analyses place halide hopping in the range expected from theory and show that iodide-bromide mixing markedly increases the rate of bulk halide transport.

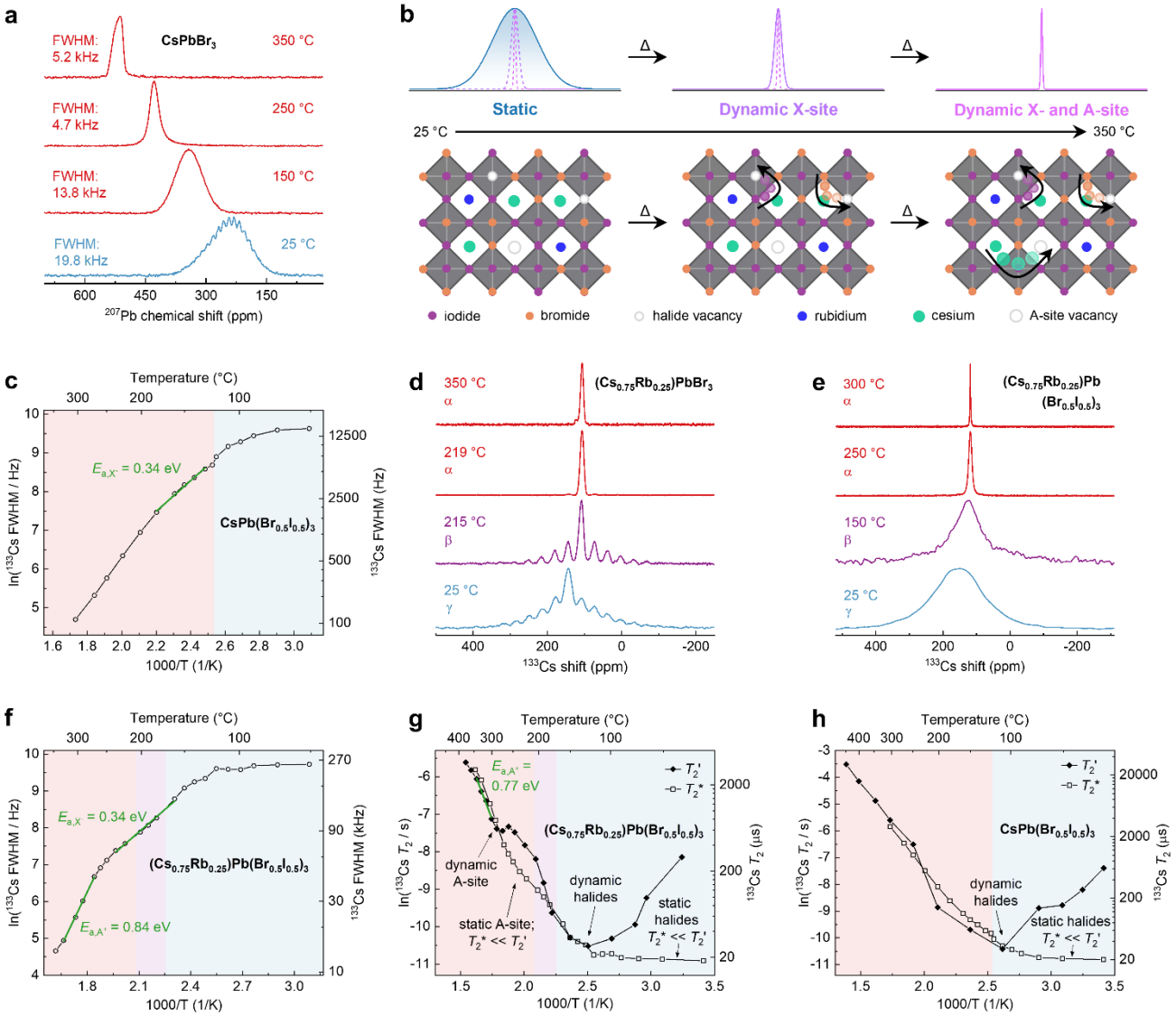

Fig. 2. Revealing and quantifying compositional dependence of halide and A-site ion diffusion by MAS NMR. (**a**) Variable temperature ^{207}Pb MAS NMR spectra (20.0 T, 4 kHz) of $CsPbBr_3$. (**b**) Schematic showing structural origin of motional averaging regimes leading to spectral narrowing at elevated temperatures. (**c**) ^{133}Cs linewidth analysis of $CsPb(Br_{0.5}I_{0.5})_3$. Variable-temperature ^{133}Cs MAS NMR spectra (20.0 T, 4 kHz) of $(Cs_{0.75}Rb_{0.25})PbBr_3$ (**d**) and $(Cs_{0.75}Rb_{0.25})Pb(Br_{0.5}I_{0.5})_3$ (**e**). (**f**) ^{133}Cs linewidth analysis of $(Cs_{0.75}Rb_{0.25})Pb(Br_{0.5}I_{0.5})_3$. Arrhenius plots of ^{133}Cs T_2' relaxation time constants for $(Cs_{0.75}Rb_{0.25})Pb(Br_{0.5}I_{0.5})_3$ (**g**) and $CsPb(Br_{0.5}I_{0.5})_3$ (**h**).

To probe the slower A-site process more directly, we measure ^{133}Cs spin-spin (T_2') relaxation. Unlike linewidth narrowing, T_2' analysis does not require full motional averaging of static disorder, making it especially useful for sluggish diffusion. In the doubly mixed composition (simultaneous Cs/Rb and I/Br mixing), T_2' exhibits two minima: a lower and higher temperature one, which we attribute, respectively, to halide hopping and A-site cation hopping (**Fig. 2g**). The latter yields an activation energy of 0.77 eV, close to that obtained from linewidth analysis (0.84 eV), confirming that A-site migration becomes accessible only at substantially higher temperatures than halide diffusion. In $CsPb(Br_{0.5}I_{0.5})_3$, by contrast, only the lower-temperature minimum is observed within the accessible temperature window, indicating that without Rb^+ substitution A-site vacancies remain much less mobile (**Fig. 2h**). Collectively, the linewidth, T_1, and T_2' analyses show that halide and A-site diffusion can be distinguished, that halide diffusion is primarily governed by X-site composition, and that A-site diffusion depends on both X- and A-site composition.

Importantly, these NMR measurements permit an estimate of intrinsic bulk halide diffusivity (**Supplementary Note S5**).[25,26] Extrapolating the high-temperature motional correlation times using the Arrhenius model gives a room-temperature diffusion coefficient of order 10^{-11} cm^2 s^{-1} for the mixed-halide compositions. Because this extrapolation

spans structural phase transitions, we treat the value as an order-of-magnitude estimate rather than a direct room-temperature measurement. It nevertheless lies below the 10^{-8}–10^{-9} cm^2 s^{-1} range commonly inferred from electrical measurements of thin films.[27–31] Those measurements include contributions from grain boundaries, interfaces, and other defect-rich pathways,[11–15] whereas MAS NMR is sensitive to atomic motion within the bulk perovskite phase. Macroscopic transport coefficients should therefore not be interpreted as intrinsic bulk diffusivities without accounting for composition and microstructure.

Molecular Dynamics Reproduces Composition-Dependent Ion Mobility

To rationalize the experimentally observed trends, we perform large-scale molecular dynamics simulations for the same composition series, together with $CsPbI_3$, using a machine-learned interatomic potential trained to describe defect formation and migration (**Supplementary Note S6**).[32] The calculations use a fixed vacancy concentration and therefore compare mobility per available defect rather than equilibrium defect populations. Within this constraint, they reproduce the qualitative experimental trends and the separation between halide and A-site diffusion timescales.

For halides, the lowest diffusivities occur in the end-member bromide and iodide materials, whereas either A- or X-site mixing promotes overall halide diffusivity, with combined A- and X-site mixing giving the highest overall halide diffusion (**Fig. 3a**). For A-site cation transport, the compositional dependence is even more pronounced: mixed A-site and mixed-halide chemistry together produce the most rapid A-site cation diffusion, whereas $CsPbBr_3$ displays the lowest diffusivity (**Fig. 3b**). The simulations also reproduce the large separation between halide and A-site timescales seen by NMR, with halides consistently diffusing much faster than A-site cations, by a factor of around 10^3. This result rationalizes the line narrowing and T_1/T_2' reduction observed in NMR as indeed corresponding to ionic motion. Arrhenius fitting results in vacancy-mediated ion hopping activation energies comparable to those found experimentally by NMR (**Fig. 3c**).

The simulations also shed light on which ions dominate transport in mixed-ion perovskites. In bromide-iodide compositions, iodide diffuses more readily than bromide, partly accounting for the enhanced overall halide transport relative to pure $CsPbBr_3$ (**Fig. 3a**). However, counterintuitively, $CsPbI_3$ does not show the fastest halide diffusion; instead, its diffusivity is comparable to that of $CsPbBr_3$ and lower than that of the mixed-halide materials. This observation rules out a simple monotonic picture in which diffusion is determined only by larger anion size or weaker average Pb-X bonding. Likewise, on the A-site, Rb^+ diffuses more rapidly than Cs^+ in mixed-A-site compounds, but the simulations show that Cs^+ mobility also increases in the compositionally mixed materials (**Fig. 3b**). Thus, neither average lattice contraction nor steric crowding alone can explain the trends.

To identify the origin of these trends, we compare structural factors that change upon ion mixing, including bond strengths, dynamic disorder, steric constraints along migration pathways, and static local distortions (**Supplementary Note S6**). Within this composition series, static local distortion shows the strongest association with enhanced mobility. Mixing broadens the distribution of local environments and creates a low-barrier subset of migration pathways that is absent from the compositionally uniform end members. Composition therefore changes not only the average structure or mean hopping barrier, but also the distribution of pathways available to a mobile defect. This explains why the mixed compositions can exhibit greater diffusivity even when their average activation energies change only modestly.

These findings refine rather than overturn previous reports of ion migration in compositionally mixed perovskites. Electrical measurements have shown reduced migration barriers and increased mobile-ion densities in mixed-halide films, while recent machine-learned molecular dynamics simulations predict enhanced halide-defect diffusion in $CsPb(I/Br)_3$. At first sight, enhanced intrinsic mobility may appear inconsistent with the suppressed photoinduced phase segregation reported for closely related Rb/Cs–Br/I compositions. The quantities are different: our simulations compare mobility at fixed vacancy concentration, whereas macroscopic segregation additionally depends on equilibrium defect abundance, interfaces, and the thermodynamic or photoinduced driving force. Operational stability therefore cannot be inferred from per-defect mobility alone.

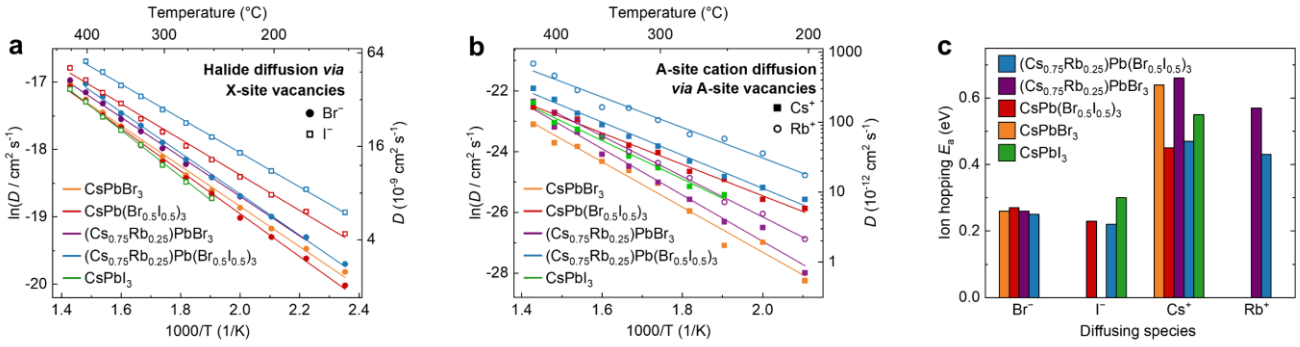

Fig. 3. Machine-learned molecular dynamics simulations rationalize composition dependence of ion diffusivity. Arrhenius plots showing temperature dependence of diffusion coefficients of halides diffusing in a model containing 1% X-site vacancies (**a**) and A-site cations diffusing in a model containing 1% A-site vacancies (**b**). (**c**) Activation energies extracted from Arrhenius fitting in panels a and b for halide and A-site cation diffusion.

Compositional mixing therefore has several distinct consequences. It changes the intrinsic mobility of an existing defect by reshaping its local migration landscape, while also influencing defect formation, phase thermodynamics, and microstructure. These effects need not vary in the same direction. The present measurements isolate the first contribution, showing that the ion-mixing strategies used to control bandgap and phase stability also modify bulk phonon behavior and per-defect ion mobility. Variable-temperature MAS NMR thus provides a means of evaluating intrinsic dynamics independently of the interfaces and defect populations that often dominate device-scale measurements.

In summary, variable-temperature MAS NMR combined with machine-learned molecular dynamics separates soft-phonon behavior, halide diffusion, and A-site cation diffusion in compositionally disordered halide perovskites. The central insight is not that disorder is uniformly beneficial or detrimental, but that it broadens the local migration landscape and creates pathways with substantially different mobilities. Distinguishing mobility per available defect from defect concentration and macroscopic driving forces provides a more rigorous basis for relating atomic-scale dynamics to processing and operational stability in multicomponent ionic semiconductors.

ASSOCIATED CONTENT

Detailed experimental procedures, characterization data and details of computational methods. This material is available free of charge via the Internet at http://pubs.acs.org.

AUTHOR INFORMATION

Corresponding Author

Dominik J. Kubicki – *School of Chemistry, University of Birmingham, Edgbaston, Birmingham, B15 2TT, UK*; https://orcid.org/0000-0002-9231-6779; Email: d.j.kubicki@bham.ac.uk

Author Contributions

Conceptualization: BMG, DJK
Methodology: BMG, DJK, JW, PE
Investigation: BMG, PD, SB, EF, JH, MW, JD, WB, PE
Visualization: BMG, DJK
Funding acquisition: DJK, BMG, JW, PE
Project administration: BMG, DJK
Supervision: DJK, JW, PE
Writing – original draft: BMG, DJK
Writing – review & editing: BMG, PD, SB, EF, JH, MW, WB, PE, JW, DJK

Funding Sources

DJK, BMG, SB, LS and MW acknowledge UKRI Horizon Europe guarantee grant EP/Y01376*X*/1 (PhotoPeroNMR) and Engineering and Physical Sciences Research Council grants EP/T015063/1 and EP/R029946/1. BMG is grateful to also receive funding *via* HORIZON EUROPE (Marie Skłodowska-Curie Action Postdoctoral Fellowship) grant 101153827 (GreenPeroInk). PD, EF, JW and PE are grateful for support from the following: Swedish Strategic Research Foundation's Future Research Leader program (FFL21-0129) (PD, JW), Swedish Energy Agency grant 45410-1 (PE), Swedish Research Council grants 2018-06482, 2019-03993 and 2020-04935 (EF, PE, JW), European Research Council Starting Grant 101162195 (JW), the Knut and Alice Wallenberg Foundation grants 2023.0032 and 2024.0042 (EF, PE, JW). Computations enabled by resources provided by the National Academic Infrastructure for Supercomputing in Sweden (NAISS) at C3SE, PDC, and NSC, partially funded by the Swedish Research Council grant 2022-06725 (PD, EF, PE, JW)

REFERENCES

1. Wang, Z.; Zeng, L.; Zhu, T.; Chen, H.; Chen, B.; Kubicki, D. J.; Balvanz, A.; Li, C.; Maxwell, A.; Ugur, E.; et al. Suppressed Phase Segregation for Triple-Junction Perovskite Solar Cells. *Nature* **2023**, *618*, 74–79.
2. McMeekin, D. P.; Sadoughi, G.; Rehman, W.; Eperon, G. E.; Saliba, M.; Hörantner, M. T.; Haghighirad, A.; Sakai, N.; Korte, L.; Rech, B.; et al. A Mixed-Cation Lead Mixed-Halide Perovskite Absorber for Tandem Solar Cells. *Science* **2016**, *351*, 151–155.
3. Shen, X.; Gallant, B. M.; Holzhey, P.; Smith, J. A.; Elmestekawy, K. A.; Yuan, Z.; Rathnayake, P. V. G. M.; Bernardi, S.; Dasgupta, A.; Kasparavičius, E.; et al. Chloride-Based Additive Engineering for Efficient and Stable Wide-Bandgap Perovskite Solar Cells. *Adv. Mater.* **2023**, *35*, 2211742.
4. Gallant, B. M.; Holzhey, P.; Smith, J. A.; Choudhary, S.; Elmestekawy, K. A.; Caprioglio, P.; Levine, I.; Sheader, A. A.; Hung, E. Y.-H.; Yang, F.; et al. A Green Solvent Enables Precursor Phase Engineering of Stable Formamidinium Lead Triiodide Perovskite Solar Cells. *Nat. Commun.* **2024**, *15*, 10110.
5. Macpherson, S.; Doherty, T. A. S.; Winchester, A. J.; Kosar, S.; Johnstone, D. N.; Chiang, Y.-H.; Gałkowski, K.; Anaya, M.; Frohna, K.; Iqbal, A. N.; et al. Local Nanoscale Phase Impurities Are Degradation Sites in Halide Perovskites. *Nature* **2022**, *607*, 294–300.
6. Othman, M.; Jeangros, Q.; Rothmann, M. U.; Jiang, Y.; Ballif, C.; Hessler-Wyser, A.; Wolff, C. M. Linking Nanoscopic Insights to Millimetric-Devices in Formamidinium-Rich Perovskite Photovoltaics. *Adv. Mater.* **2025**, *37*, 2409742.
7. Hu, S.; Wang, J.; Zhao, P.; Pascual, J.; Wang, J.; Rombach, F.; Dasgupta, A.; Liu, W.; Truong, M. A.; Zhu, H.; et al. Steering Perovskite Precursor Solutions for Multijunction Photovoltaics. *Nature* **2025**, *639*, 93–101.
8. Zheng, L.; Wei, M.; Eickemeyer, F. T.; Gao, J.; Huang, B.; Gunes, U.; Schouwink, P.; Bi, D. W.; Carnevali, V.; Mensi, M.; et al. Strain-Induced Rubidium Incorporation into Wide-Bandgap Perovskites Reduces Photovoltage Loss. *Science* **2025**, *388*, 88–95.
9. Fransson, E.; Rosander, P.; Eriksson, F.; Rahm, J. M.; Tadano, T.; Erhart, P. Limits of the Phonon Quasi-Particle Picture at the Cubic-to-Tetragonal Phase Transition in Halide Perovskites. *Commun. Phys.* **2023**, *6*, 173.
10. Thiesbrummel, J.; Milić, J. V.; Deibel, C.; Garnett, E. C.; Tao, S.; Kirchartz, T.; Guerrero, A.; Cameron, P.; Tress, W.; Islam, M. S.; et al. Ion Migration in Perovskite Solar Cells. *Nat. Rev. Chem.* **2026**, *10*, 179–195.
11. Yun, J. S.; Seidel, J.; Kim, J.; Soufiani, A. M.; Huang, S.; Lau, J.; Jeon, N. J.; Seok, S. I.; Green, M. A.; Ho-Baillie, A. Critical Role of Grain Boundaries for Ion Migration in Formamidinium and Methylammonium Lead Halide Perovskite Solar Cells. *Adv. Energy Mater.* **2016**, *6*, 1600330.
12. Ćavar, L. D.; Schütz, E. R.; Yalçinkaya, Y.; Bach, C.; Deibel, C.; Schmidt-Mende, L.; Weber, S. A. L. Resolving Ionic Spectra of Lead-Halide Perovskites to the Nanometer. *Nanoscale* **2026**, *18*, 8263–8277.
13. Biega, R.-I.; Leppert, L. Halogen Vacancy Migration at Surfaces of CsPbBr3 Perovskites: Insights from Density Functional Theory. *J. Phys. Energy* **2021**, *3*, 034017.
14. Meggiolaro, D.; Mosconi, E.; De Angelis, F. Formation of Surface Defects Dominates Ion Migration in Lead-Halide Perovskites. *ACS Energy Lett.* **2019**, *4*, 779–785.

15. Samatov, M. R.; Liu, D.; Zhao, L.; Kazakova, E. A.; Abrameshin, D. A.; Das, A.; Vasenko, A. S.; Prezhdo, O. V. Ion Migration at Metal Halide Perovskite Grain Boundaries Elucidated with a Machine Learning Force Field. *J. Phys. Chem. Lett.* **2024**, *15*, 12362–12369.
16. Thiesbrummel, J.; Le Corre, V. M.; Peña-Camargo, F.; Perdigón-Toro, L.; Lang, F.; Yang, F.; Grischek, M.; Gutiérrez-Partida, E.; Warby, J.; Farrar, M. D.; et al. Universal Current Losses in Perovskite Solar Cells Due to Mobile Ions. *Adv. Energy Mater.* **2021**, *11*, 2101447.
17. Thiesbrummel, J.; Shah, S.; Gutiérrez-Partida, E.; Zu, F.; Peña-Camargo, F.; Zeiske, S.; Diekmann, J.; Ye, F.; Peters, K. P.; Brinkmann, K. O.; et al. Ion-Induced Field Screening as a Dominant Factor in Perovskite Solar Cell Operational Stability. *Nat. Energy* **2024**, *9*, 664–676.
18. Kubicki, D. J.; Stranks, S. D.; Grey, C. P.; Emsley, L. NMR Spectroscopy Probes Microstructure, Dynamics, and Doping of Metal Halide Perovskites. *Nat. Rev. Chem.* **2021**, *5*, 624–645.
19. Kruszyńska, J.; Ebic, M.; Gallant, B. M.; Kubicki, D. J.; Nawrocki, J.; Yadav, P.; Akin, S.; Prochowicz, D. Solvated Palladium (II) Complexes for Efficient and Stable All-Inorganic CsPbI2Br Perovskite Solar Cells. *Small* **2026**, *22*, e14110.
20. Malyshkin, D.; Sereda, V.; Ivanov, I.; Mazurin, M.; Sednev-Lugovets, A.; Tsvetkov, D.; Zuev, A. New Phase Transition in CsPbBr3. *Mater. Lett.* **2020**, *278*, 128458.
21. Šimėnas, M.; Balčiūnas, S.; Wilson, J. N.; Svirskas, S.; Kinka, M.; Garbaras, A.; Kalendra, V.; Gągor, A.; Szewczyk, D.; Sieradzki, A.; et al. Suppression of Phase Transitions and Glass Phase Signatures in Mixed Cation Halide Perovskites. *Nat. Commun.* **2020**, *11*, 5103.
22. Šimėnas, M.; Gągor, A.; Banys, J.; Mączka, M. Phase Transitions and Dynamics in Mixed Three- and Low-Dimensional Lead Halide Perovskites. *Chem. Rev.* **2024**, *124*, 2281–2326.
23. Eames, C.; Frost, J. M.; Barnes, P. R. F.; O'Regan, B. C.; Walsh, A.; Islam, M. S. Ionic Transport in Hybrid Lead Iodide Perovskite Solar Cells. *Nat. Commun.* **2015**, *6*, 7497.
24. Yantara, N.; Mathews, N. Toolsets for Assessing Ionic Migration in Halide Perovskites. *Joule* **2024**, *8*, 1239–1273.
25. Griffith, K. J.; Seymour, I. D.; Hope, M. A.; Butala, M. M.; Lamontagne, L. K.; Preefer, M. B.; Koçer, C. P.; Henkelman, G.; Morris, A. J.; Cliffe, M. J.; et al. Ionic and Electronic Conduction in TiNb2O7. *J. Am. Chem. Soc.* **2019**, *141*, 16706–16725.
26. Stanje, B.; Rettenwander, D.; Breuer, S.; Uitz, M.; Berendts, S.; Lerch, M.; Uecker, R.; Redhammer, G.; Hanzu, I.; Wilkening, M. Solid Electrolytes: Extremely Fast Charge Carriers in Garnet-Type Li6La3ZrTaO12 Single Crystals. *Ann. Phys. (Berlin)* **2017**, *529*, 1700140.
27. Li, C.; Guerrero, A.; Huettner, S.; Bisquert, J. Unravelling the Role of Vacancies in Lead Halide Perovskite through Electrical Switching of Photoluminescence. *Nat. Commun.* **2018**, *9*, 5113.
28. Yang, T.-Y.; Gregori, G.; Pellet, N.; Grätzel, M.; Maier, J. The Significance of Ion Conduction in a Hybrid Organic–Inorganic Lead-Iodide-Based Perovskite Photosensitizer. *Angew. Chem., Int. Ed.* **2015**, *54*, 7905–7910.
29. McGovern, L.; Futscher, M. H.; Muscarella, L. A.; Ehrler, B. Understanding the Stability of MAPbBr3 versus MAPbI3: Suppression of Methylammonium Migration and Reduction of Halide Migration. *J. Phys. Chem. Lett.* **2020**, *11*, 7127–7132.
30. Reichert, S.; Flemming, J.; An, Q.; Vaynzof, Y.; Pietschmann, J.-F.; Deibel, C. Ionic-Defect Distribution Revealed by Improved Evaluation of Deep-Level Transient Spectroscopy on Perovskite Solar Cells. *Phys. Rev. Appl.* **2020**, *13*, 034018.
31. Armaroli, G.; Maserati, L.; Ciavatti, A.; Vecchi, P.; Piccioni, A.; Foschi, M.; Van der Meer, V.; Cortese, C.; Feldman, M.; Foderà, V.; et al. Photoinduced Current Transient Spectroscopy on Metal Halide Perovskites: Electron Trapping and Ion Drift. *ACS Energy Lett.* **2023**, *8*, 4371–4379.
32. Deswal, P. et al. Vacancy migration in mixed halide perovskites. *To be published*.